PROGRESS IN EDDY CURRENT MODELING VIA THE BOUNDARY ELEMENT METHOD

N. Nakagawa, S. Ghanekar, D. Lehther, Y. Liu, J. C. Moulder,
and A. N. S. Prasad
Center for NDE
Iowa State University, Ames, IA 50011

F. Rizzo
Dept. of Aerospace Engineering and Engineering Mechanics
Iowa State University, Ames, IA 50011

J. C. Chao
United Technologies, Pratt & Whitney
P. O. Box 109600, West Palm Beach, FL 33410-9600

INTRODUCTION

For the past several years, we have been developing an eddy current model, using the boundary element method (BEM). Last year, in particular, a BEM algorithm based on the Hertz potential approach was found and shown to be effective in dealing with complex part geometry, while keeping the computational resource requirement to a minimum [1-3]. This paper concerns a further extension of the model to include cracks.

To recapitulate our overall objective [1-2], our task is to develop the so-called "measurement models", *i.e.* theoretical models of probe-flaw interactions, applicable to existing and newly developed inspection systems. The model is then implemented into software, so that one can analyze given inspection problems on computers, predict inspection performances, design probes [4], and make possible improvements.

To meet this objective, the scope of the model capabilities should be fairly general, requiring conceptual eddy current inspection systems (Fig. 1) to include coils, (ferrite) cores, parts, and any number of those in arbitrary shapes. The coils and cores may be assembled to form a complicated probe design of absolute and/or differential types. The part and defect geometry may be as complicated as a crack on edge.

To the best of our knowledge, the BEM is the most suitable numerical technique to the task, striking the right balance between the required geometrical flexibility and limited computational resources [1-2]. We have demonstrated also that, among various possible BEM formulations of electromagnetism, the Hertz potential approach is the most

Review of Progress in Quantitative Nondestructive Evaluation. Vol. 16
Edited by D.O. Thompson and D.E. Chimenti, Plenum Press, New York, 1997

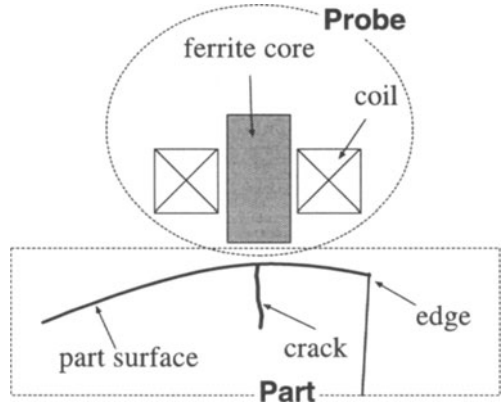

Figure 1. Illustration for a schematic eddy current inspection system. The proposed modeling algorithm allows the introduction of ferrite cores with minimal expense. It makes no assumptions on object geometry.

economical computationally, while being able to handle geometrical singularities such as edges adequately [1-4], without requiring any special treatment of edge nodes [5].

The model capabilities presented last year included most of the required features, except, primarily, for the crack model. Adding the crack modeling capability is therefore the focus of this paper. The following section contains a brief account of how the crack modeling has been formulated. In the subsequent section, we present example predictions of impedance signals and their comparison with experimental data. The last section is for conclusions.

FORMULATION

General Technical Approach

As described in Introduction, our goal is to perform computer simulation of EC inspections. On the one hand, we need to solve Maxwell equations in complex geometry to achieve the objective. On the other hand, we wish to limit our computer platform to engineering workstations from the economical consideration. To satisfy both demands, we select the boundary element method.

Also, we need the maximum flexibility in manipulating probe and part geometry. To this end, we have interfaced the BEM code to commercial CAD packages, and the approach has been found satisfactory. On the CAD package, one can perform tasks such as part geometry creation, probe design, mesh generation, and scan plan generation.

3D EC BEM Model

We describe the modeling algorithm here only briefly, partly because the Hertz potential formulation was described before [1-4], and partly because we plan to publish the detail elsewhere.

It suffices to state that the BEM casts the basic partial differential equations plus boundary conditions into a set of simultaneous integral equations, which then are solved numerically via the standard element method. The procedure involves the use of Green's functions that helps to reduce the unknown degrees of freedom to surface fields only.

Last year, we reported a version of the BEM approach to electromagnetism via the Hertz potentials [1-3]. We first introduced the magnetic scalar potential ψ, and wrote the magnetic field $\vec{H}$ in air and ferrite cores as

$$\vec{H} = \vec{H}^0 + \vec{\nabla}\psi \,. \tag{1}$$

We next expressed the electric ($\vec{E}$) and magnetic fields in conductors as

$$\vec{E} = \sigma^{-1}\vec{\nabla}\times\vec{\Pi}\,, \quad \vec{H} = \vec{\Pi} + \vec{\nabla}\Psi \tag{2}$$

where $\vec{\Pi}, \Psi$ = Hertz vector and scalar potentials [6]. (In Refs. 1-4, $\vec{\Pi}$ was written as $\vec{h}$.) Equation (1) simplifies the problem substantially in air and core, while the symmetry between Eqs. (1) and (2) makes the continuation from air to metal straightforward. It should be noted, in passing, that we do not use the impedance boundary condition, which breaks down at the edge-like geometrical singularities. (See, e.g, Ref. 5.)

All necessary formulas may be found in Refs. 1-4, except for the reciprocity formula for the probe impedance calculation. The formula with the magnetic scalar potential may be found in Ref. 7 for a single coil case. For differential and reflection probes, the formula must be generalized to multiple coils (Fig. 2), analogous to the one in Ref. 8. The resulting formula reads,

$$\Delta Z_{21} = \frac{-i\omega\mu_0}{I_1 I_2}\int_S dS\,\vec{n}\cdot\left[\chi_2\vec{\nabla}(\chi_1' - \chi_1) - (\chi_1' - \chi_1)\vec{\nabla}\chi_2\right] \tag{3}$$

where Z_{21} = transition impedance from coil 1 to coil 2, ΔZ_{21} = its change due to a flaw, I_α = current strength ($\alpha = 1,2$), $\vec{H}_\alpha = \vec{\nabla}\chi_\alpha$ in the vicinity of S, and the un-primed [primed] quantities are those in the absence [presence] of the flaw.

Crack Modeling Algorithm

We will next mention the key features of our crack modeling algorithm.

First, we use the effective source description of defects. Namely, the presence of a defect is described mathematically by an equivalent source (denoted by $\vec{s}$ in Fig. 3),

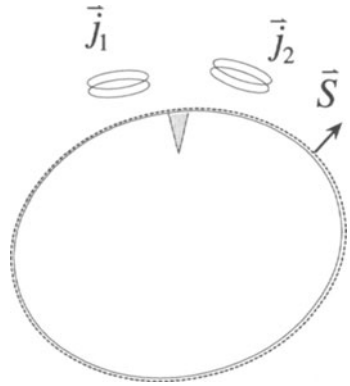

Figure 2. Illustration for the part object and EC coils for which the reciprocity formula (3) is written. Although not drawn here, any number of core objects can appear in addition.

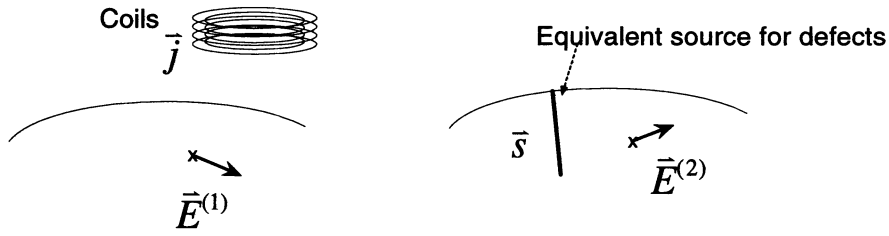

Figure 3. The equivalent source description of the defect. The electric field $\vec{E}^{(2)}$, generated by the source $\vec{s}$ at the defect position, cancels the incident field $\vec{E}^{(1)}$, so that $E_n^{(1)} + E_n^{(2)} = 0$ on the crack surface.

instead of changing the part geometry explicitly. The defect source generates the electric field $\vec{E}^{(2)}$, which is added to the coil-induced incident field $\vec{E}^{(1)}$. The source $\vec{s}$ is the basic unknown, to be determined from the cancellation condition so that $E_n^{(1)} + E_n^{(2)} = 0$ on the crack surface.

Second, we assume the crack to be tightly closed. Accordingly, we take the first moment $\langle \vec{s} \rangle$ of the source $\vec{s}$ with respect to the width direction. In the tight crack limit, the only remaining component is $\langle s_n \rangle (\equiv \varphi)$. Then, in terms of the Bowler potential φ, the above cancellation condition can be expressed as

$$-E_n^{inc} = \int_{S_c} dS \left[\overline{\overline{G}}_{nn} \varphi \right] + \vec{n}_P \cdot \int_S dS \left[\left(\vec{\nabla} G \right) \times \left(\vec{n} \times \vec{E} \right) - \{ \cdots \} \right], \tag{4}$$

where the r.h.s. is the crack-induced field ($E_n^{(2)}$), in which the first term is the direct term while the second represents the surface reflection.

Third, we exploit the fact that, in Eq. (4), the potential φ generates the field at its own location. We therefore saturate the r.h.s. of Eq. (4) by the most singular part of the direct term. Under this approximation (or the contact approximation), Eq. (4) reduces to

$$0 = E_n^{inc} + \int_{S_c} dS \left[\left(-\partial_t^2 G \right) \varphi \right], \tag{5}$$

which determines φ with the appropriate regularization of the singular kernel [9]. Having determined φ, one can finally compute the crack signal from φ and E_n^{inc} via the reciprocity formula [9]. Incidentally, the function G in Eqs. (4) and (5) is the usual scalar Green's function in the medium.

PREDICTED CRACK SIGNALS AND COMPARISON WITH EXPERIMENT

In this section, we present two sets of example computations and their comparison with experimental data. The first example is about edge crack signals relative to flat-surface crack signals. The second example concerns an absolute comparison of theory with experiment using an edge crack specimen.

Flat-Surface vs. Edge Cracks

Here, we compare two different types of cracks on Ti-6Al-4V specimens (conductivity = $6.1\times10^5\ S/m$), one on a flat surface (length x depth = 0.99 mm x 0.33 mm) and the other at the straight edge (length x depth = 3.75 mm x 0.375 mm). (See the illustration in Fig. 4.) The probe used here is a commercial probe, which is absolute and axi-symmetric but otherwise its internal parameters are unknown. We therefore used the equivalent coil description. Namely, we determined equivalent coil parameters as given in Fig. 4, so that computed crack signals reproduce the measurement data approximately for the flat-surface case (Fig. 5A). Given the effective coil parameters, we then computed the edge crack signals, and compared the results with the measurement data. Figure 5B shows the comparison of the absolute values of the probe impedance.

Figure 4. Illustration of the dimensions of the equivalent coil and the cracks. (A) is for the flat-surface crack, which is semi-elliptical of the length 0.99 mm with the aspect ratio 3 to 1. (B) The edge crack is a rectangular EDM notch. The coil parameters are determined empirically from the flat-surface data (Fig. 5A below). See the text for details.

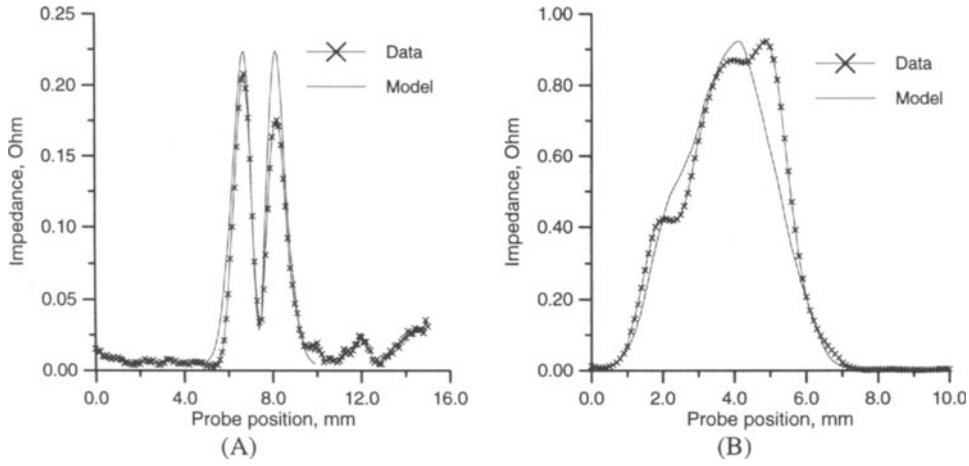

Figure 5. Probe impedance plots vs. probe positions. (A) is for the flat-surface crack. This is a fit from which the coil parameters shown in Fig. 4 are determined. (B) is the result of the comparison between the data and the prediction from the coil parameters thus determined.

Edge and Edge Crack Signals

The second example provides an absolute test for the computation because the coil parameters are known: the inner diameter = 1.07 mm, the outer diameter = 2.62 mm, the coil length = 2.93 mm, and the built-in lift off = 0.62 mm, with 235 turns. The probe was operated at 500 kHz. The specimen is made of Ti-6Al-4V and the EDM notch dimensions are $l \times d \times w = 3.84mm \times 0.384mm \times 0.11mm$. Figure 6 illustrates these dimensions. Figure 7 shows the impedance plots as functions of probe positions. In this example, both the edge signals (Fig. 7A) and the crack signals (Fig. 7B) are shown. In both cases, the probe starts from a on-metal position, move across the straight edge, and eventually go off the edge. Plotted in Fig. 7A are the probe impedance changes when there is no defect under the probe path. The coil still picks up large signals due to the geometry (edge). When the scan path happens to go over the crack, the probe impedance changes by an extra amount due to the crack, in addition to the edge signals. Experimentally, therefore, it is necessary to subtract the edge signals from the measured total impedance, in order to obtain the crack

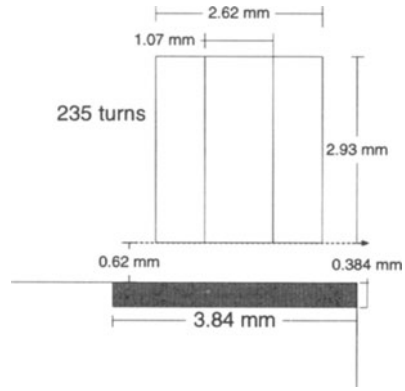

Figure 6. Illustration to indicate the dimensions of the crack and the coil, and their relative positions. The coil scans over the crack, parallel to the length direction.

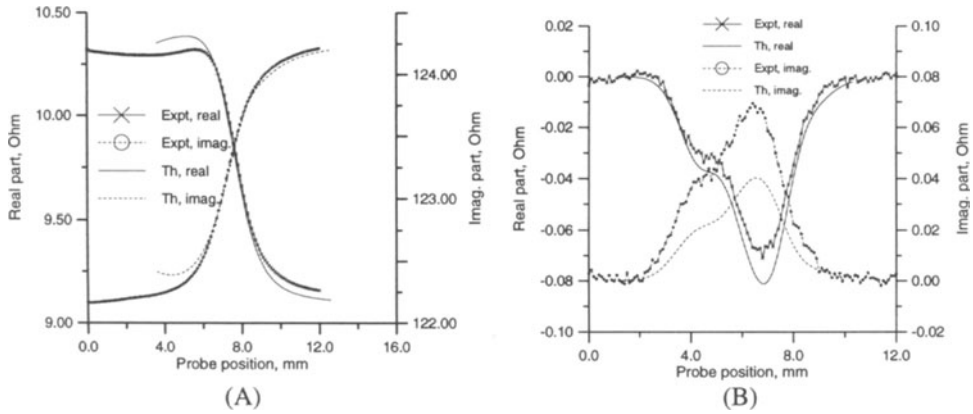

Figure 7. Impedance plots vs. probe position. The coil is on metal when the position is 0.0, and goes off the edge as the position value increases. The computed results and the experimental data (both real and imaginary parts) are plotted together. (A) is the edge signals, *i.e.* when the coil is away from the crack. (B) corresponds to the crack signals, *i.e.* the total impedance minus the edge signals.

signals plotted in Fig. 7B. Notice that the crack signals are an order of magnitude smaller than the edge signals. Computationally, the reciprocity formula provides the way to compute the small quantity (the crack signal ΔZ) directly in terms of the Bowler potential.

The results of Figs. 5 and 7 indicate the quality of agreements achieved by the present model. Specifically, the results in Fig. 5 demonstrate that, by using the model, any empirical knowledge about crack signals obtained with simple flat-surface specimens can be extrapolated fairly accurately to more complex geometry cases such as edge cracks. Notice that measurements with flat-surface specimens do not yield any information about geometry signals. The model can fill this gap by predicting geometry signals as in Fig. 7A, provided that the internal probe parameters are known. Finally, the absolute comparison in Fig. 7B appears to be encouraging. Clearly, the agreement of the real parts is satisfactory,[1] and so is the magnitude. The origin of the discrepancy in the imaginary parts is yet to be verified. It is likely, however, that the deviation will decrease if the volume effect of the EDM notch is properly taken into account.

CONCLUSIONS

This paper reports on the progress in the general 3D eddy current inspection model based on the BEM and the Hertz potential description. Specifically, a crack modeling algorithm has been developed and implemented into a software module. The module, then, has been incorporated into the previously developed incident-field code [1-3]. The combined code has yielded crack impedance predictions as shown in Figs. 5 and 7. From the numerical results presented there, we conclude (1) that the code has succeeded in yielding reasonable crack signal predictions for the selected problems at the accuracy of ~10% level, and (2) that the model can be used, even in its present form, to address practical problems such as extrapolating empirical knowledge about crack signals obtained with simple block specimens to crack detections in complex geometry such as holes and slots with edges.

We believe that the model capabilities established to date are sufficiently encouraging, and thus plan to continue the development toward completion by further validating the code and add possible refinements. We also plan to incorporate the model into a software simulator to promote the model use toward industrial applications [10]. Specific application areas include aircraft engine components (fan disk inspections) and nuclear power plants (heat-exchanger tubing).

ACKNOWLEDGMENTS

This work was supported by the Program for Integrated Design, NDE and Manufacturing Sciences under U.S. Department of Commerce, National Institute of Standards and Technology Cooperative Agreement No. 70NANB4H1535. This work was also supported in part by the Engine Titanium Consortium under the Federal Aviation Administration Grant No. 94-G-048, and in part by the NSF Industry/University Cooperative Research Program.

[1] It should be noted here that there was an error in the crack code which yielded the crack impedance that was too small by a factor 2, as reported at the Conference. The code has been corrected since, yielding the results shown in Fig. 7B.

REFERENCES

1. N. Nakagawa, J. Chao, and A. N. S. Prasad, "In-Service Eddy Current Inspection and Computer Simulation," in *Nondestructive Testing of Materials*, eds. R. Collins, W. D. Dover, J. R. Bowler, and K. Miya (IOS Press, 1995), p. 203.
2. N. Nakagawa and J. C. Chao, in *Review of Progress in QNDE*, Vol. 15, eds. D. O. Thompson and D. E. Chimenti (Plenum, New York, 1996), p. 339.
3. J. Chao, D. Lehther, J. C. Moulder and N. Nakagawa, in *Review of Progress in QNDE*, Vol. 15, eds. D. O. Thompson and D. E. Chimenti (Plenum, New York, 1996), p. 355.
4. J. Chao, A. N. S. Prasad, N. Nakagawa, and D. Raulerson, in *Review of Progress in QNDE*, Vol. 15, eds. D. O. Thompson and D. E. Chimenti (Plenum, New York, 1996), p. 1105.
5. E. M. Deeley, IEEE Trans. Magn. 28, 2814 (1992).
6. J. A. Stratton, *Electromagnetic Theory* (McGraw-Hill, New York, 1949).
7. R. E. Beissner, Rev. Prog. QNDE, vol. 8, 229-236, 1989; B. A. Auld, S. R. Jefferies, and J. C. Moulder, J. Nondestruct. Eval. 7: 79-94 (1988).
8. B. A. Auld, J. C. Moulder, S. Jefferies, P. J. Shull, S. Ayter, and J. Kenney, Res. Nondestr. Eval. 1, 1 (1989).
9. N. Nakagawa, in *Review of Progress in QNDE*, Vol. 8, eds. D. O. Thompson and D. E. Chimenti (Plenum, New York, 1989), p. 245.
10. N. Nakagawa, M. Garton, J. C. Moulder, J. H. Rose, and J. Xu, "Recent Development of Eddy Current Inspection Simulator," in *Review of Progress in QNDE*, this volume.